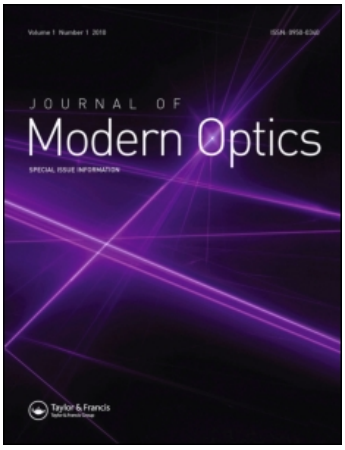

Journal of Modern Optics
Publication details, including instructions for authors and subscription information:
http://www.informaworld.com/smpp/title~content=t713191304

Signatures of carrier multiplication in the frequency resolved fluorescence spectra from polaritons

Oleksiy Roslyak[a]; Godfrey Gumbs[b]; Shaul Mukamel[a]
[a] Chemistry Department, University of California, Irvine, CA 92697-2025, USA [b] Physics and Astronomy Department, Hunter College, CUNY, NY 10065, USA

First published on: 13 September 2010

To cite this Article Roslyak, Oleksiy , Gumbs, Godfrey and Mukamel, Shaul(2010) 'Signatures of carrier multiplication in the frequency resolved fluorescence spectra from polaritons', Journal of Modern Optics, 57: 19, 2009 — 2019, First published on: 13 September 2010 (iFirst)
To link to this Article: DOI: 10.1080/09500340.2010.499048
URL: http://dx.doi.org/10.1080/09500340.2010.499048

Journal of Modern Optics
Vol. 57, No. 19, 10 November 2010, 2009–2019

Signatures of carrier multiplication in the frequency resolved fluorescence spectra from polaritons

Oleksiy Roslyak[a]*, Godfrey Gumbs[b] and Shaul Mukamel[a]

[a]*Chemistry Department, University of California, Irvine, CA 92697-2025, USA;* [b]*Physics and Astronomy Department, Hunter College, CUNY, NY 10065, USA*

(*Received 8 March 2010; final version received 17 May 2010*)

Using the micro-cavity coupled to weakly confined excitons in quantum dots we investigated the signatures of carrier multiplication in the single and two-photon emitted frequency resolved fluorescence. Those are compared to the spectra provided by the conventional multi-photon induced fluorescence. The two processes are distinguished by the statistics of the initial polariton distribution. We argue that exciton emission spectra turned out to be CM insensitive, while the polaritons emission demonstrates strong spectral signatures of the CM. When the polaritonic effect dominates the confinement-boosted excitons' nonlinearities, increasing quantum yield leads to consecutive appearance of Rabi multiplets. The correlation spectra reveal the formation of more multiplets as compared to the single photon emission. When the confinement increases the multiplets start to overlap and their classification requires transient measurements of the spectral snapshots. These are based on the discrete Auger lifetimes of the multi-excitons.

Keywords: carrier multiplication; multi-excitons; bi-exciton; 2D spectroscopy; nano-crystal quantum dots

1. Introduction

One of the most important mechanisms for producing multiple electron-hole pairs (multiexcitons) per absorbed photon is carrier multiplication (CM) [1–3]. In a typical transient experiment (either absorption of photo-luminescence), a pump photon of energy well above the excitonic threshold, e.g. $\hbar\omega = 3E_g$, creates high energy carriers whose inelastic scattering creates multiple electron/hole pairs (excitons), thus efficiently harvesting the photon energy. Competition from another ultrafast inter-band relaxation mechanism results in a small CM efficiency in bulk semiconductors [4,5]. For instance, the rate of impact ionization must compete with the rate of energy relaxation by electron-phonon scattering. Aside from this effect, the threshold photon energy for impact ionization exceeds that required for the conservation of energy alone because, in addition, the crystal momentum must be conserved. It has been shown that the rate of impact ionization overwhelms photon scattering rate when the kinetic energy of the pump excited electron is many times the bandgap energy.

In contrast to the bulk, in quantum dots (QDs), some of the processes are suppressed or enhanced due to the discrete energy structure. The carriers' confinement eliminates the need for crystal momentum conservation. The 'phonon bottleneck' effect reduces the phonon-assisted relaxation rate and increased electron–hole Coulomb interaction greatly enhances the rate of Auger cooling process,[1] including the inverse Auger process[2] of impact ionization. Multiple experiments show that the later mechanism is the primary source of CM in QDs [6]. Some other mechanism of CM, such as coherent superposition and direct photoionization had been also proposed (see [7] and references therein).

TA measurements capitalize on the pump-induced absorption changes in the probe, which are primarily attributed to the Coulomb interactions [4,8]. The average exciton multiplicity produced by CM is usually followed by the Auger recombination of the multi-excitons manifold. The measure of impact ionization induced CM is quantum yield (QY), which shows how many electron–hole pairs can be harvested from a pump photon of given energy. For TA experiments the CM-induced changes in the probe absorption suggest that a single photon could generate up to seven $e-h$ pairs (OY = 700%) in PbSe and that CM is similarly efficient in visible-emitting CdSe nanocrystals [1,6]. The QY linearly depends on the pump photon energy (after a certain energy threshold).

However, the formation of more complicated $e-h$ complexes such as unstable bi-exciton may drastically change the Auger rate. The QD environment and

*Corresponding author. Email: avroslyak@gmail.com

ISSN 0950–0340 print/ISSN 1362–3044 online

DOI: 10.1080/09500340.2010.499048
http://www.informaworld.com

growth methods may produce strong quenching effect on the QY [9]. The quenching mechanism is unclear so far. Moreover, some recent transient photo-luminescence (TP) spectroscopy experiments performed on CdSe and CdTe nano-crystals showed no CM, and no bi-exciton and exciton signatures in TP decays were reported [8,9]. TP is especially sensitive to the competing relaxation mechanisms since it utilizes one of them (exciton radiative recombination) as the measurement. Nevertheless, the most straightforward explanation of both types of the transient signals is based on the deviation of the multi-exciton statistics in the QDs from the Poisson distribution characteristic to the multi-photon induced photoluminescence [1,10]. Alternatively, a model based on the exciton spectral density was proposed in [11]. An even more sophisticated explanation of CM dynamics based on a series of odd-ordered inter-band scattering events was developed in [7].

To clarify this discrepancy between the TA and TP results, and the large variation of the reported QY, it would be useful to identify additional techniques that may reveal signatures of CM-induced multiexcitons in QDs. The most straightforward method would be to try to look at the frequency resolved photoluminescence spectra [12–15]. However, such a schematic suffers from the fact that the biexciton effect is masked by the various dephasing and relaxation mechanisms. Additional observed resonances are attributed to the high exciton manifolds once the saturation of the lowest manifold is reached. This requires a high pump flux, which is usually not the case in the solar cells since the pump there is continuous rather than the pulses. Some important semiconductors, such as lead salts, even have large saturation limits due to the specifics of their electronic structure. Moreover, as we demonstrate in this paper, even if one would be able to significantly lower the dephasing so that it becomes possible to observe multiexcitons of the same kind (1S), the resulting spectra would not be sensitive to the CM mechanism of the multiexciton formation. That is, the same time of the spectra would be produced by conventional multi-photon induced photoluminescence. Recall that the latter relies on the probability of the QD simultaneously absorbing more the one photon.

Here, we propose to look at the CM fluorescence[3] from the QD placed into a microcavity [16–18]. It might seem that introduction of the microcavity and the polaritonic effect may be an overhead for even as such complicated theory. However, we shall show that this makes the spectra sensitive not only to the number of the particles but also to the specifics of the mechanism the particles had been formed. We demonstrate this by comparing the multi-photon and CM-induced fluorescence from the lowest (1S) excitons coupled to a microcavity. Analogously to the photoluminescence spectra from the multi-excitons (1S-1S, 1P-1P) [14] the polariton spectra are defined by various levels (angular momentum) and sub-levels (projection of the angular momentum) [19], but the resonances are highly sensitive to the QY. Even more sensitivity to CM demonstrates two-photon correlation fluorescence spectra (in the sense of Glauber two-photon counting) [20]. The paper is organized as follows. The next section introduces the model of bosonized QD excitons coupled to the microcavity. The resultant polaritonic states in the angular momentum representation are calculated using first-order perturbation with respect to the Coulomb and phase-filling nonlinearities. The third section treats the coupling to the free (measured) field perturbatively in the light-matter interaction, thus defining single and two-photon fluorescence. The specifics of the initial state of the system is also discussed there. The final section presents some numerical simulations and discussion.

2. Model

In this article we propose the following experimental setup to observe some signatures of the carrier multiplication. A collection of $\mathcal{N}$ identical noninteracting semiconducting QDs are dissolved into a layer of transparent polymer host [16]. Each QD is assumed to be large enough to assume weak electron/hole confinement. The QD-confining potential effectively restrains the motion of the exciton center of mass as well as the boosted Coulomb interaction due to reduced carrier screening. That is, the electron/hole wavefunctions spill out of QD to the host material with, usually, a much smaller dielectric constant. QD must be able to accommodate at least four lowest excitons of the same kind. This will allow us to neglect possible saturation effects and the signatures of multi-excitons formed by various types of excitons.

Lead salts (PbS, PbSe and PbTe) quantum dots [21] of radius more than 10 nm are good candidates for our model. These have direct band gaps (for PbSe, $E_g = 0.28\,\mathrm{eV}$) at four equivalent L points in the Brillouin zone. The bottom of the conduction band has L_6^- symmetry in the double group notation, and the top of the valence band has L_6^+ symmetry [22]. Spatially, the valence band-edge Bloch functions are s–like, while the conduction band-edge Bloch functions are $p_{\langle 111\rangle}$−like, where $\langle 111\rangle$ denotes the direction in the cubic lattice. Therefore, the transitions are optically active and may be described by the transition dipole moment μ_{cv}.

Excitons in quantum dots are assumed to be strongly coupled to the cavity central mode, thus forming polaritons. The microcavity is made either of Bragg stacked mirrors [16] or a recently proposed photonic crystal nano-cavity [18,17]. The polaritons, in turn, are weakly coupled to the free field modes via their excitonic part. Initially, the polaritons as well as free optical field modes are in the vacuum state. The system (microcavity + quantum dots) is then illuminated with strong laser pump pulses of central frequency $\hbar\omega_p > 3E_g$. Such a way of polariton population is going to is usually referred to as transient setup. The time separation between the consequent pulses is much large than the exciton lifetime. Due to weak interaction between the polaritons and the free fields, the latter photon population changes. The change can be homodyne detected via single- and two-photon fluorescence techniques as shown in Figure 1.

The detectors are equipped with the gates allowing us to measure the spectral snapshot of the transient signal. The gates are turned on at time t_0 for a few periods of the measured mode, thus allowing us to measure the time integrated frequency resolved spectra.

One way to calculate the fluorescence signals is using the sum over states mode [20]. It requires mapping from the polaritons to excitations of a collection of $\mathcal{N}$ artificial atoms, whose energy levels and transition selection rules are known. Such mapping will be our first step. At any initial time t_0 the system of QD weakly interacting excitons strongly coupled with microcavity field and weakly coupled to the free field modes is assumed to be in

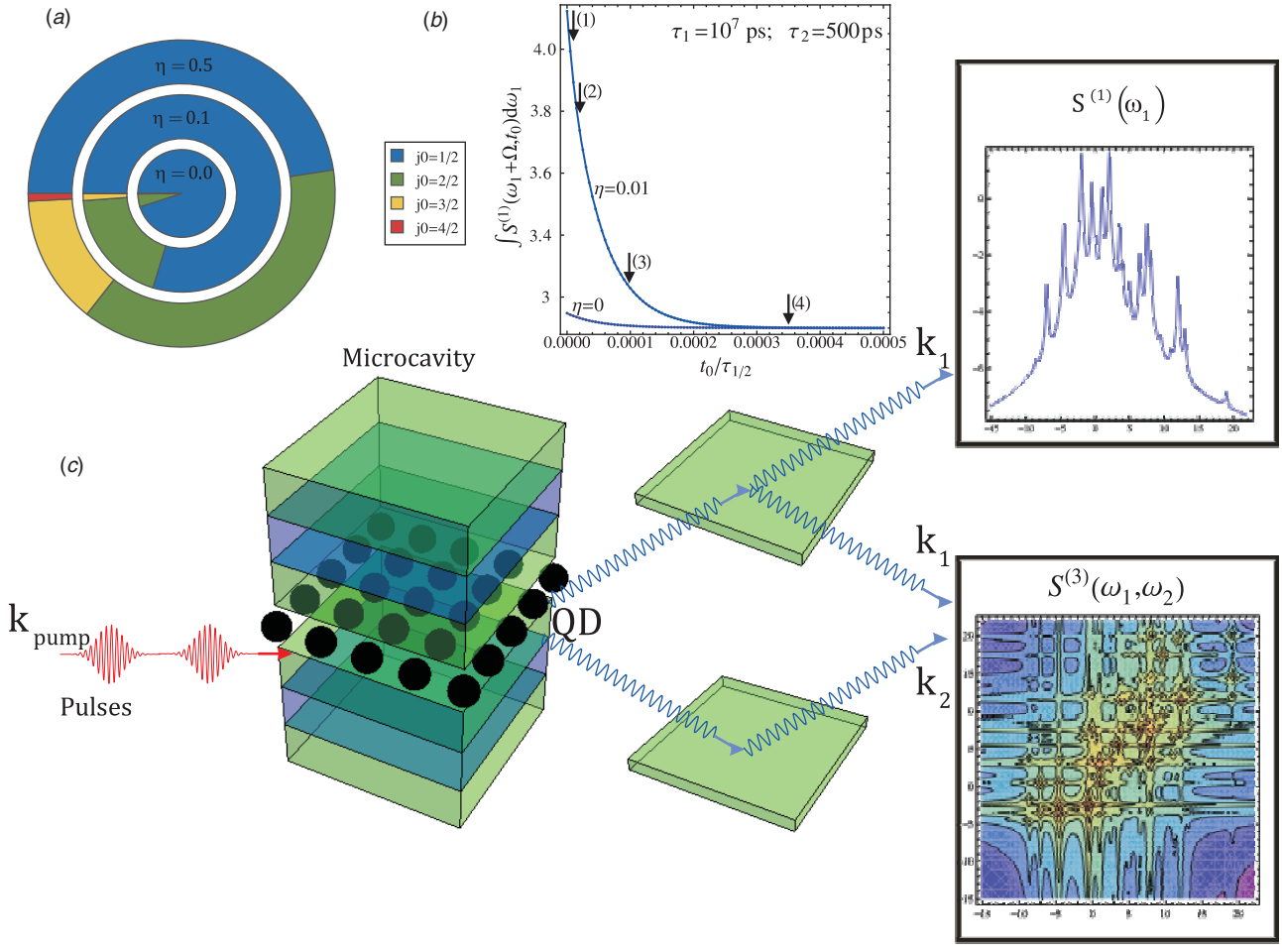

Figure 1. Transient single and two-photon florescence from the polariton states populated by CM. (*a*) Relative contribution of the multi-polariton states to the fluorescence signal at $t0 = 0$ for various values of the CM defining phenomenological parameter η. (*b*) Frequency integrated single photon transient fluorescence spectra. The arrows indicate the spectral snapshots when the discrete Auger process reduces the contribution from multi-polariton states to the signal. These are used for classifying the spectral resonances in case of large nonlinearities. (*c*) Schematics of the proposed experiment. (The color version of this figure is included in the online version of the journal.)

quasi-equilibrium and its evolution can be described by the following Hamiltonian [23–33]:

$$\begin{aligned} H &= H_{\mathrm{sys}} + H_{\mathrm{int}}(t-t_0) \\ H_{\mathrm{sys}} &= \hbar\omega_C a^\dagger a + \hbar\omega_{1S} B^\dagger B + \hbar G\left(a^\dagger B + B^\dagger a\right) \\ &\quad + \hbar g B^\dagger B^\dagger B B \\ H_{\mathrm{int}}(t) &= -\mu_{1S}\sum_i \left[E_i(t)B^\dagger + E_i^\dagger(t)B\right]. \end{aligned} \tag{1}$$

Here ω_C is the central frequency of the microcavity mode; $a^\dagger(a)$ are the creation (annihilation) operators for the cavity photons, which obey bosonic commutation relation $[a, a^\dagger]=1$; $\hbar\omega_{1S}$ is the lowest exciton energy. We define QD excitons by means of its creation operator [26]:

$$B_n^\dagger = \frac{1}{\sqrt{V}}\sum_{\mathbf{k},\sigma}\phi_n^\star(M\mathbf{k})e_{\mathbf{k},\sigma}^\dagger h_{-\mathbf{k},\sigma'}^\dagger \tag{2}$$

where we have confined ourselves to the case of zero exciton momentum; $M=(m_h^\star - m_e^\star)/(m_h^\star + m_e^\star)$ with $m_e^\star(m_h^\star)$ being the effective mass of electron (hole); $e^\dagger(h^\dagger)$ is the electron (hole) creation operators; $\phi_n(M\mathbf{k})$ is their relative motion envelop function in the momentum space; $\sigma(\sigma')$ span the quantum numbers related to the confinement as well as spin variables; V is the quantum dot volume. We shall consider the lowest ($n=1S$) excitons, thus omitting the subscript for the creation operator (2). In this case the envelop function has the simplified form: $\phi_{1S}(M\mathbf{k}) = 8(\pi a_{1S}^3)^{1/2}/(1+M^2k^2a_{1S}^2)$, where a_{1S} is the exciton radius.

The interaction between the cavity and the exciton is given by the factor:

$$\hbar G = \sqrt{\frac{2\pi\hbar\omega_c}{\Omega_C}}\mu_{1S} \tag{3}$$

where we introduced the exciton transition dipole moment $\mu_{1S} = V^{-1/2}\mu_{cv}\sum_{\mathbf{k}}\phi_{1S}(M\mathbf{k})$.

Parameter g represents an effective interaction between excitons and depends on the confinement degree. For the given Coulomb interaction between the confined electron and hole $V(\mathbf{q}) = 4\pi e^2/(\epsilon_0 q^2)$, with ϵ_0 being the static dielectric constant, the interaction between the excitons in the quantum dot has the form:

$$\begin{aligned} \hbar g = -\frac{2}{V^3}\sum_{\mathbf{k},\mathbf{k}'} & V(M(\mathbf{k}-\mathbf{k}'))\left|\phi_{1S}(M\mathbf{k})\right|^2 \\ & \times\left[\left|\phi_{1S}(M\mathbf{k}')\right|^2 - \phi_{1S}(M\mathbf{k})\phi_{1S}^\star(M\mathbf{k}')\right]. \end{aligned} \tag{4}$$

Here we assume that the interaction is a positive real number, which means that the multi-exciton complexes are not stable.

The last term in Equation (1) is written in the interaction picture with respect to the free field Hamiltonian [27]. It is determined by the electric field annihilation operator for the ith free field mode $E_i(t) = \sqrt{\frac{2\pi\hbar\omega_i}{\Omega_i}}a_i\exp(-i\omega_i t)$, where a_i annihilates a photon in the mode; Ω_i is the mode quantization volume; ω_i is its frequency.

Owing to the non-bosonic nature of the exciton operator (2) the system Hamiltonian in its current form is not well suited for our discussion. To deal with that problem we represent the system Hamiltonian in terms of effective bosonic operators. One of the bosonization procedures has been proposed by Usui [28]:

$$B^\dagger = b^\dagger - \nu b^\dagger b^\dagger b, \quad \left[b, b^\dagger\right] = 1. \tag{5}$$

Here, we introduced the phase-space filling factor [26]:

$$\nu = \frac{1}{V}\frac{\sum_{\mathbf{k}}\left|\phi_{1S}(M\mathbf{k})\right|^2\phi_{1S}(M\mathbf{k})}{\sum_{\mathbf{k}}\phi_{1S}(M\mathbf{k})}. \tag{6}$$

The merit of Usui transformation is that the transformed Hamiltonian may be split into an ideal bosonic part H_0 and the part H_1 describing their weak interaction:

$$\begin{aligned} H_{\mathrm{sys}} &= H_0 + H_1 \\ H_0 &= \hbar\omega_c a^\dagger a + \hbar\omega_{1S} b^\dagger b + \hbar G\left(a^\dagger b + b^\dagger a\right) \\ H_1 &= \hbar g b^\dagger b^\dagger b b - \hbar\nu G\left(a^\dagger b^\dagger b b + b^\dagger b^\dagger a b\right). \end{aligned} \tag{7}$$

The first term in H_1 deals with the deviation of the excitons from ideal bosons, thus correcting for the excitonic density effects. The second term describes an additional nonlinear interaction via the cavity mode.

Now let us turn to the problem of finding eigenvectors and eigenvalues of the system Hamiltonian (7). It is convenient to give the solution of the non-perturbed Hamiltonian H_0 using Schwinger's angular momentum representation of bosonic operators [19,29]. The angular momentum operators are defined as:

$$2\hat{J}_x = a^\dagger b + b^\dagger a, \quad 2i\hat{J}_y = a^\dagger b - b^\dagger a \tag{8}$$

$$2\hat{J}_z = a^\dagger a - b^\dagger b, \quad \hat{J}^2 = \frac{\hat{N}}{2}\left(\frac{\hat{N}}{2}+1\right) \tag{9}$$

where $\hat{N} = a^\dagger a + b^\dagger b$ is the total number of particles operator.

The Hamiltonian can now be written in terms of SO(3) rotations

$$H_0 = \hbar\Omega\hat{N} + \hbar A e^{-i\theta\hat{J}_y}\hat{J}_z e^{i\theta\hat{J}_y}. \tag{10}$$

Here we have introduced some auxiliary quantities

$$\Omega = \frac{1}{2}(\omega_C + \omega_{1S}) \quad \Delta = \omega_C - \omega_{1S} \tag{11}$$

$$A = \sqrt{\left(\Delta^2 + 4G^2\right)} \quad \tan\theta = \frac{2G}{\Delta}. \tag{12}$$

For fixed number of polaritons N, the eigenvectors and eigenvalues of the above Hamiltonian are dressed exciton states:

$$\left|\psi_{j,m}^{(0)}\right\rangle = \exp\left(-i\theta\hat{J}_y\right)|j,m\rangle \tag{13}$$

$$E_{j,m}^{(0)} = \hbar(N\Omega + mA) \tag{14}$$

$$a|j,m\rangle = \sqrt{j+m}\,|j-1/2, m-1/2\rangle \tag{15}$$

$$b|j,m\rangle = \sqrt{j-m}\,|j-1/2, m+1/2\rangle. \tag{16}$$

Here, the common eigenstates of $\hat{J}^2$ and $\hat{J}_z$ are the Fock states with $j+m$ photons in the cavity and $j-m$ excitons in the quantum dot, respectively:

$$|j,m\rangle = \frac{\left(a^\dagger\right)^{j+m}\left(b^\dagger\right)^{j-m}}{\sqrt{(j+m)!(j-m)!}}|0\rangle \tag{17}$$

with $j=N/2$, and $m=N/2,\ldots,-N/2$. Using the Baker–Hausdorff identity we obtain the matrix elements of the cavity photon and exciton in the polaritonic basis:

$$\begin{aligned}
a^\star_{j,m;j',m'} &= \langle\psi^{(0)}_{jm}|a^\dagger|\psi^{(0)}_{j'm'}\rangle \\
&= \delta_{j',j-\frac{1}{2}}\left[\delta_{m',m-\frac{1}{2}}\sqrt{j+m}\cos\frac{\theta}{2}\right. \\
&\quad \left. -\,\delta_{m',m+\frac{1}{2}}\sqrt{j-m}\sin\frac{\theta}{2}\right] \\
b^\star_{j,m;j',m'} &= \langle\psi^{(0)}_{jm}|b^\dagger|\psi^{(0)}_{j'm'}\rangle \\
&= \delta_{j',j-\frac{1}{2}}\left[\delta_{m',m+\frac{1}{2}}\sqrt{j-m}\cos\frac{\theta}{2}\right. \\
&\quad \left. +\,\delta_{m',m-\frac{1}{2}}\sqrt{j+m}\sin\frac{\theta}{2}\right] \\
a_{j,m;j',m'} &= \langle\psi^{(0)}_{jm}|a|\psi^{(0)}_{j'm'}\rangle \\
&= a^\star_{j',m';j,m} \\
b_{j,m;j',m'} &= \langle\psi^{(0)}_{jm}|b|\psi^{(0)}_{j'm'}\rangle = b^\star_{j',m';j,m}.
\end{aligned} \tag{18}$$

Using Equation (18) we can calculate perturbative part of the system Hamiltonian in the polariton basis:

$$\begin{aligned}
&\langle\psi^{(0)}_{jm}|H_1|\psi^{(0)}_{j'm'}\rangle \\
&= \sum_{m1=-j'+1/2}^{j'-1/2}\sum_{m2=-j'+1}^{j'-1}\sum_{m3=-j'+1/2}^{j'-1/2}\left[\hbar g b^\star_{j,m;j'-1/2,m3}\right. \\
&\quad \times b^\star_{j'-1/2,m3;j'-1,m2}b_{j'-1,m2;j'-1/2,m1}b_{j'-1/2,m1;j',m'} \\
&\quad -\hbar\nu G a^\star_{j,m;j'-1/2,m3}b^\star_{j'-1/2,m3;j'-1,m2} \\
&\quad \times b_{j'-1,m2;j'-1/2,m1}b_{j'-1/2,m1;j',m'} \\
&\quad -\hbar\nu G b^\star_{j,m;j'-1/2,m3}b^\star_{j'-1/2,m3;j'-1,m2} \\
&\quad \left.\times a_{j'-1,m2;j'-1/2,m1}b_{j'-1/2,m1;j',m'}\right].
\end{aligned} \tag{19}$$

The perturbed Hamiltonians (7) are given by:

$$\begin{aligned}
E_{j,m} &= E^{(0)}_{j,m} + \langle\psi^{(0)}_{j,m}|H_1|\psi^{(0)}_{j,m}\rangle \\
&= \hbar\Omega N + \hbar A m + \frac{1}{4}\hbar g(5j^2 - 3j + m^2) \\
&\quad -\frac{1}{4}(j^2 + j - 3m^2)(\hbar g\cos 2\theta + \hbar\nu\sin 2\theta) \\
&\quad - m(2j-1)(\hbar g\cos\theta - \hbar\nu\sin\theta).
\end{aligned} \tag{20}$$

The corresponding eigenvectors have the form:

$$|\psi_{j,m}\rangle = |\psi^{(0)}_{j,m}\rangle + \sum_{m1\neq m}\frac{\langle\psi^{(0)}_{j,m}|H_1|\psi^{(0)}_{j,m1}\rangle}{E^{(0)}_{j,m} - E^{(0)}_{j,m1}}|\psi^{(0)}_{j,m1}\rangle. \tag{21}$$

Utilizing Equations (19) and (21) we can calculate the transition selection rules to the first order in parameters g and ν, obtaining:

$$\begin{aligned}
\mu^\star_{j,m;j,m'} &= \mu_{1S}\langle\psi_{j,m}|B^\dagger|\psi_{j',m'}\rangle \\
&= \mu_{1S}\langle\psi^{(0)}_{j,m}|B^\dagger|\psi^{(0)}_{j',m'}\rangle \\
&\quad + \mu_{1S}\sum_{m1\neq m'}\frac{\langle\psi^{(0)}_{j',m1}|H_1|\psi^{(0)}_{j',m'}\rangle}{E^{(0)}_{j',m'} - E^{(0)}_{j',m1}}b^\star_{j,m;j',m1}.
\end{aligned} \tag{22}$$

Here the unperturbed transition matrix element has the form:

$$\begin{aligned}
&\langle\psi^{(0)}_{j,m}|B^\dagger|\psi^{(0)}_{j',m'}\rangle \\
&\quad = b^\star_{j,m;j',m'} - \hbar\nu\sum_{m2=-j'}^{j'}\sum_{m1=-j'+1/2}^{j'-1/2}b^\star_{j,m;j',m2} \\
&\qquad \times b^\star_{j',m2;j'-1/2,m1}b_{j'-1/2,m1;j',m'}.
\end{aligned} \tag{23}$$

Aside from the specifics of the dephasing mechanism, the polariton eigenvalues (20) and transition dipole moments (22) are the only necessary ingredients for calculating the fluorescence signals with sum-over-states formalism. This is the subject of the next section.

3. Fluorescence from CM versus photoinduced polaritons

In the following approach, developed in [27,30] we assume that each of our two photon detectors can measure the rate of change of the number of photons in the given free field[4] mode ω_1 within a time frame $(t-t_0)$:

$$S_1(t,t_0) = \int_{t_0}^{t}\frac{\mathrm{d}}{\mathrm{d}\tau}\langle a_1^\dagger a_1\rangle_{t_0}\mathrm{d}\tau. \tag{24}$$

In the beginning of the measurement t_0, the free field is assumed to be in its vacuum state, thus making our experiment setup equivalent to those of Glauber photon counting. Notation $\langle\cdots\rangle_{t_0}$ means averaging over the initial state of the system (polaritons + free field). The signal can be calculated perturbatively

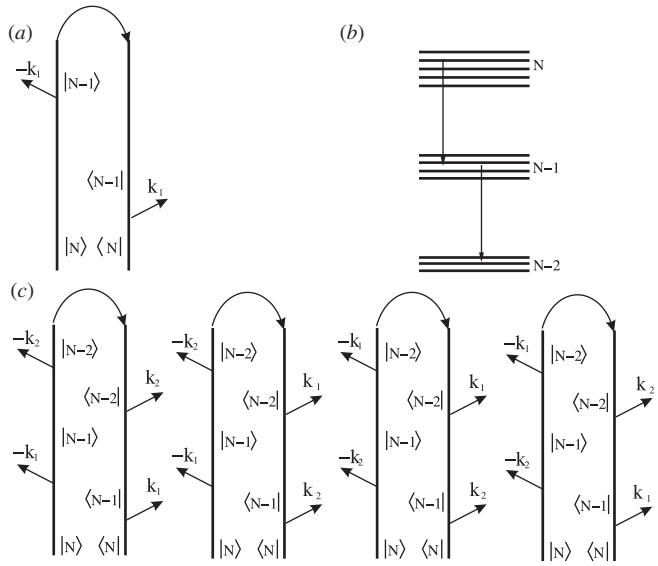

Figure 2. CTPL diagrams ([30] MARX) for (*a*) one-photon and (*b*) two-photon fluorescence. (*c*) Level scheme of polaritons. The arrows indicate transitions between the levels (sub-levels selection rules are not shown).

to desired order. CTPL diagrams provide a convenient framework for such expansion. Single photon counting can be described by the CTPL diagram shown in Figure 2(*a*).

Using the loop diagram rules in [27,30] the single-photon fluorescence can be written as:

$$S^{(1)}(\omega_1) = \mathcal{N}\frac{2\pi\hbar\omega_1}{\Omega}\,\mathrm{Im}\sum_{j0,m0}|\langle\psi(t_0)|\psi_{j0,m0}\rangle|^2 \times\left[\frac{i}{\hbar}\langle\psi_{j0,m0}|B^{\dagger}G_{\{j0,m0\}(\omega_1)}B|\psi_{j0,m0}\rangle\right]. \quad (25)$$

Here, $|\psi(t_0)\rangle$ is the initial state of the system,and $G(\omega)$ ($G^{\dagger}(\omega)$) is the retarded (advanced) propagator given by:

$$G_{\{j0,m0\}(\omega)}\omega = i\hbar\sum_{jm}\frac{|\psi_{j,m}\rangle\langle\psi_{j,m}|}{\hbar\omega + E_{j0,m0} - E_{j,m} + i\hbar\gamma} \quad (26)$$

where γ is the dephasing rate of the corresponding transition. Here we assume that it is mostly defined by the quality of the cavity $Q = E_C/\hbar\gamma$.

Using the transition selection rules in Equation (22), the single-photon fluorescence can be written as:

$$S^{(1)}(\omega_1) = \mathcal{N}\frac{2\pi\hbar\omega_1}{\Omega_1}\,\mathrm{Im}\sum_{j0}\sum_{m0=-j0}^{j0}\sum_{m1=-j0+1/2}^{j0-1/2}P(j0,m0) \times|\mu_{j0,m0;j0-1/2,m1}|^2 G^{\star}_{j0,m0;j0-1/2,m1}(\omega_1). \quad (27)$$

Here, Green's functions are the matrix elements of the propagator in the polariton basis:

$$G_{j0,m0;j0-1/2,m1}(\omega) = \frac{\hbar}{i\hbar\omega - (E_{\{j0,m0\}} - E_{\{j0-1/2,m1\}}) + i\hbar\gamma}. \quad (28)$$

The probability of a single quantum dot having state $|\psi_{j0,m0}\rangle$ initially populated has been denoted as:

$$P(j0,m0;t_0) = |\langle\psi(t_0)|\psi_{j0,m0}\rangle|^2. \quad (29)$$

This probability once combined with the transition dipole moment $P(j0,m0;t_0)|\mu^{\star}_{j0,m0;j,m1}|^2$ determines the intensity of the spectral lines. According to Equation (22) after some straightforward algebra the levels selection rule can be written as $j0 - j = 1/2$. This simply signifies that a single photon emitted from the micro cavity reduces the number of polaritons by one. Similarly, projection of the angular momentum provides sub-level part of the transition rule. The linear part of the Hamiltonian, Equation (10), results in $m - m0 = \pm 1/2$ transitions, while its nonlinear part, Equation (19), is a source of additional transition rules: $m - m0 = \pm 3/2, \pm 5/2$.

In full analogy with the single emitted photon fluorescence we can derive the signal for the two-photon emitted fluorescence. Experimentally, it can be homodyne detected via a two-photon counting procedure when two detectors simultaneously detect a change in photon population of the two given free field modes:

$$S_{1,2}(t,t_0) = \int_{t_0}^{t}\frac{\mathrm{d}}{\mathrm{d}\tau}\langle a_1^{\dagger}a_1 + a_2^{\dagger}a_2\rangle_{t_0}\mathrm{d}\tau. \quad (30)$$

Using CTPLs in Figure 2(*c*) we can rewrite the signal above as:

$$
\begin{aligned}
&S^{(3)}(\omega_1,\omega_2;t_0)\\
&\quad=-\mathcal{N}\frac{2\pi\omega_1}{\hbar\Omega_1}\frac{2\pi\omega_2}{\hbar\Omega_2}\,\mathtt{Im}\sum_{j0}\sum_{m0=-j0}^{j0}P(j0,m0;t_0)\\
&\qquad\times\sum_{m1=-j0+1/2}^{j0-1/2}\sum_{m2=-j0+1}^{j0-1}|\mu^{\star}_{j0,m0;j0-1/2,1}\mu^{\star}_{j0-1/2,m1;j0-1,m2}|^2\\
&\qquad\times G^{\star}_{j0,m0;j0-1,m2}(\omega_1+\omega_2)|G_{j0,m0;j0-1/2,m1}(\omega_1)\\
&\qquad+G_{j0,m0;j0-1/2,m1}(\omega_2)|^2. \qquad (31)
\end{aligned}
$$

When the pump beam is off-resonance, the system usually finds itself in the mixed multi-exciton, or – as it is in our case – multi-polariton state. The specifics of of the population mechanism are all embedded into coefficients $P(j0,m0;t_0)$. We will compare conventional multi-photon induced fluorescence with fluorescence generated via the CM mechanism.

Since the energy separation between polariton sublevels is much smaller than those between the levels, we neglected the possible difference in population of the polariton sub-levels: $P(j0,m0;t_0)\rightarrow P(j0;t_0)$. This simplification allows us to use the exciton population phenomenological theory developed in [1,10] to calculate polariton population coefficients. Following their reasoning, in the case when the pump photon energy is much greater than the quantum dot energy gap E_g, carrier-induced absorption saturation is insignificant. Thus, the probability of generation of an electron/hole pair in the quantum dot is independent of the number of pairs already existing in it. When polariton states are populated by a high intensity pump beam (no CM), photoinduced-populations exhibit a Poisson distribution for which the average number of polaritons is simply proportional to the pump fluence j_p as: $\langle N_0\rangle = j_p\sigma_a$. Here, σ_a is the quantum dot absorption cross-section. The Poisson distribution of polariton populations may be written as:

$$P(j0,\langle N_0\rangle)=\frac{\langle N_0\rangle^{2j0}}{2j0}\frac{\exp(-\langle N_0\rangle)}{(2j0)!}. \qquad (32)$$

It represents the probability of having N polaritons in a selected quantum dot for a given single quantum dot for a given single exciton average population $\langle N_0\rangle$, which is an experimentally determined parameter.

The situation changes when the CM mechanism plays its role. The Poisson distribution is no longer valid and with the pump energy being in the range $3E_g<\hbar\omega p<4E_g$, we shall use the following CM-induced polariton distribution [10]:

$$
\begin{aligned}
P(j0,\langle N_0\rangle,\eta)=&\sum_{n'=\lceil 2j0/3\rceil}^{2j0-1}P(n',\langle N_0\rangle)\\
&\times\sum_{n=2j0-1}^{2n'}\eta^n(1-\eta)^{2n'-n}\frac{(2n')!}{n!(2n'-n)!}. \qquad (33)
\end{aligned}
$$

The phenomenological parameter η is related to the quantum yield as: $QY=2\eta+1$; notation $\lceil\cdots\rceil$ means taking the ceiling of the inside parameter. When $\eta=0$ the contribution from CM disappears and the signal is defined by the Poisson distribution of multi-photon induced fluorescence. Relative multi-polariton contributions for various η are illustrated in Figure 1(*b*).

It is relatively simple to modify Equations (32) and (33) to describe the transient fluorescence:

$$P(j0;t_0)=\left\{\begin{array}{c}P(j0,\langle N_0\rangle)\\ P(j0,\langle N_0\rangle,\eta)\end{array}\right\}\exp(-t_0/\tau_{j0}) \qquad (34)$$

where τ_{j0} follows from the bi-exciton τ_1 lifetime [31] as: $\tau_{j0}=\tau_1/j0^2$. These quantities describe Auger decay of the polaritons via its excitonic part.

Note that $P(j0;t_0)$ could be alternatively found using the spectral density of the multi-exciton states, as proposed in [11]. In their model, the quantum yield has the meaning of the average exciton multiplicity. However, such an approach would require multiple adjustment phenomenological parameters related to the underling relaxation mechanisms and will be reported elsewhere.

To summarize this section, the fluorescence equations, Equations (27) and (31), describe the signal and two-photon fluorescence, provided that 2D parameters (Equations (3), (4) and (6)) are known. The CM induced fluorescence is given by initial polariton distribution (Equation (32)) and will be compared with photoinduced fluorescence given by Equation (33). Various spectroscopic resonances shall be classified in accordance with corresponding polariton levels. This may be accomplished by observing the time evolution of the spectral snapshots in the transient setup using Equation (34). All the above signals will be discussed in the next section for various combinations of material parameters.

4. Numerical results and discussion

Hereafter, we shall assume the following micro-cavity parameters: the de-tuning between the exciton and the cavity mode is zero $\Delta=0$ thus making the central frequency equal to both ω_c and ω_{1S}. Their values may be approximated by the band-gap energy but since we present our graphs in the de-tuning of the emitted light

and the central frequency coordinates $\omega_1 - \Omega$ the exact value is not necessary. The quality factor is taken to be $Q = 13{,}000$ corresponding to the de-phasing rate $\gamma = 0.01\,\text{meV}$; the exciton lifetime is 10^{-7} s and the bi-exciton is 500 ps. The quantum dot is assumed to be able to accommodate at least four excitons in $1S$ lowest state. On average, only 1% of the quantum dots accept more than one photon $\langle N_0 \rangle = 0.01$, thus keeping us away from the possible saturation. This parameter fully defines Poisson statistics of multi-photon induced fluorescence. For carrier-multiplication-induced fluorescence we have to specify parameter $\eta > 0$ which varies in our simulations. Note that since we use the bosonization procedure based on Usui transformation our model is fully justified in the weak confinement regime for rather large QDs. However, it was shown in [32] that the approximation (5) is valid up to the saturation limit (q-deformed bosons approximation $q^2 = 1 - \nu$). The nonlinearity parameters must be then redefined and such regimes will be reported elsewhere.

First, we shall consider regime of strong polariton coupling (compared to the nonlinearities) when $G \gg g \gg \nu G$. We assume the following QD parameters: exciton-microcavity central mode coupling $G = 2.5\,\text{meV}$, the Coulomb matrix element $g = 0.3\,\text{meV}$ (so that $G \gg g$), the phase filling is neglected $\nu = 0$. The resulting spectra are shown in Figure 3.

In the case when CM does not play its role ($\eta = 0$, $QY = 1$) we have standard polariton emission. There are two spectral resonances (Rabi doublet) provided by a single polariton state and separated by $2G$ as shown in Figure 3(1.1). The contribution from multi-polariton states emission is too weak to be observable in a single photon emission specter. However, they show themselves in the correlation specter Figure 3(1.2). The correlation resonances shown there occur between ω_1 photon and virtual double photon $\omega_1 + \omega_2$. In accordance with Equation (31) the resonances due to ω_1 photon occur at the poles of the retarded Green's function $G_{j0,m0;j0-1/2,m1}(\omega_1)$ while the virtual double photon $\omega_1 + \omega_2$ resonances are given by the poles of the advanced Green's function across the loop $G^{\star}_{j0,m0;j0-1,m2}(\omega_1 + \omega_2)$. More precisely, the correlation between $N = 1$ (horizontal axes) and $N = 2$ (vertical axes) provide resonances arranged in a ladder-like pattern. The horizontal steps have the size of G and the vertical steps are of $2G$ size. We shall refer to such correlation resonances as group A. When the CM effect is increased to $\eta = 0.1$, $QY = 1.2$ the effect of multi-polariton emission is enhanced. The two other peaks from $N = 2$ manifold and separated by $4G$ arise as illustrated in Figure 3(2.1). They correspond to a Rabi quadruplet. The central two peaks are hidden by the Rabi doublet. The correlation specter (Figure 3(2.2)) also reveals correlation between $N = 3$ and $N = 2$ manifolds (group B). A further increase of the quantum yield ($\eta = 0.5$, $QY = 2$) reveals $N = 3$ Rabi multiplet (Figure 3(3.1)). The central peaks of which are masked by the lower multiplets. The correlation resonances between $N = 3$ and $N = 4$ polariton states appears in Figure 3(3.2). Rabi multiplets are slightly split by the Coulomb interaction.

Now let us turn to the weak coupling regime by assuming smaller size QD. Such a regime we define by the following parameters: $G = 4\,\text{meV}$ and $g = 3\,\text{meV}$. At this point we assume the phase filling $\nu = 0.1$ since it scales as $\sim 1/\text{V}$ while the Coulomb coupling scales as $\sim 1/V^{1/3}$ [29,33,23]. The spectra are given in Figure 4. Owing to to strong nonlinearities the multi-polaritons pronounce themselves even in the absence of the CM. However, their contribution is much more effective in the CM case. The Rabi multiplets become asymmetric and the emission is predominantly given by the excitonic part of the polariton manifolds. The Coulomb splitting of the multiplets is strong enough to mix up the resonances from various multiplets. To classify the resonances and correlation resonances it is convenient to use transient photoluminescence setup. We take spectroscopic snapshots at various t_0s along the Auger-driven multi-exciton relaxation as shown in the frequency integrated specter (Figure 1(b)). Due to quantized Auger lifetimes the contributions from the multi-polariton manifolds become less pronounced sequentially. That is, the contribution from $N = 4$ dies out first then $N = 3$ disappears from the spectra and so on until we are left with the Rabi doublet ($N = 2$).

The most interesting observation and the main result of this paper is that the fluorescence spectra from the excitons themselves ($G = 0$) do not show any spectral sensitivity to the CM parameter η. Even more so, this result holds true for any confinement regime above the saturation limit. With and without CM the central exciton resonance is just split into multiple exciton resonances separated by g (see Figure 4(3.1), 4(3.2)). Since for excitons $\nu G = 0$ the phase filling only modifies relative intensity of the peaks as given by Equation (23). Given a large dephasing parameter these multiexciton resonances are accountable for non-Lorentzian line shape [12]. Analogously, the polariton spectra become insensitive to the CM mechanism under increasing de-tuning Δ. On the other hand, the polariton emission spectra become more sensitive to the CM parameter η when the coupling G increases. Another merit of the proposed polariton-based fluorescence is the ability to detect signatures of the CM for the values of the pump fluence one order of magnitude smaller than those required for conventional exciton transient photoluminescence. This may be used for CM

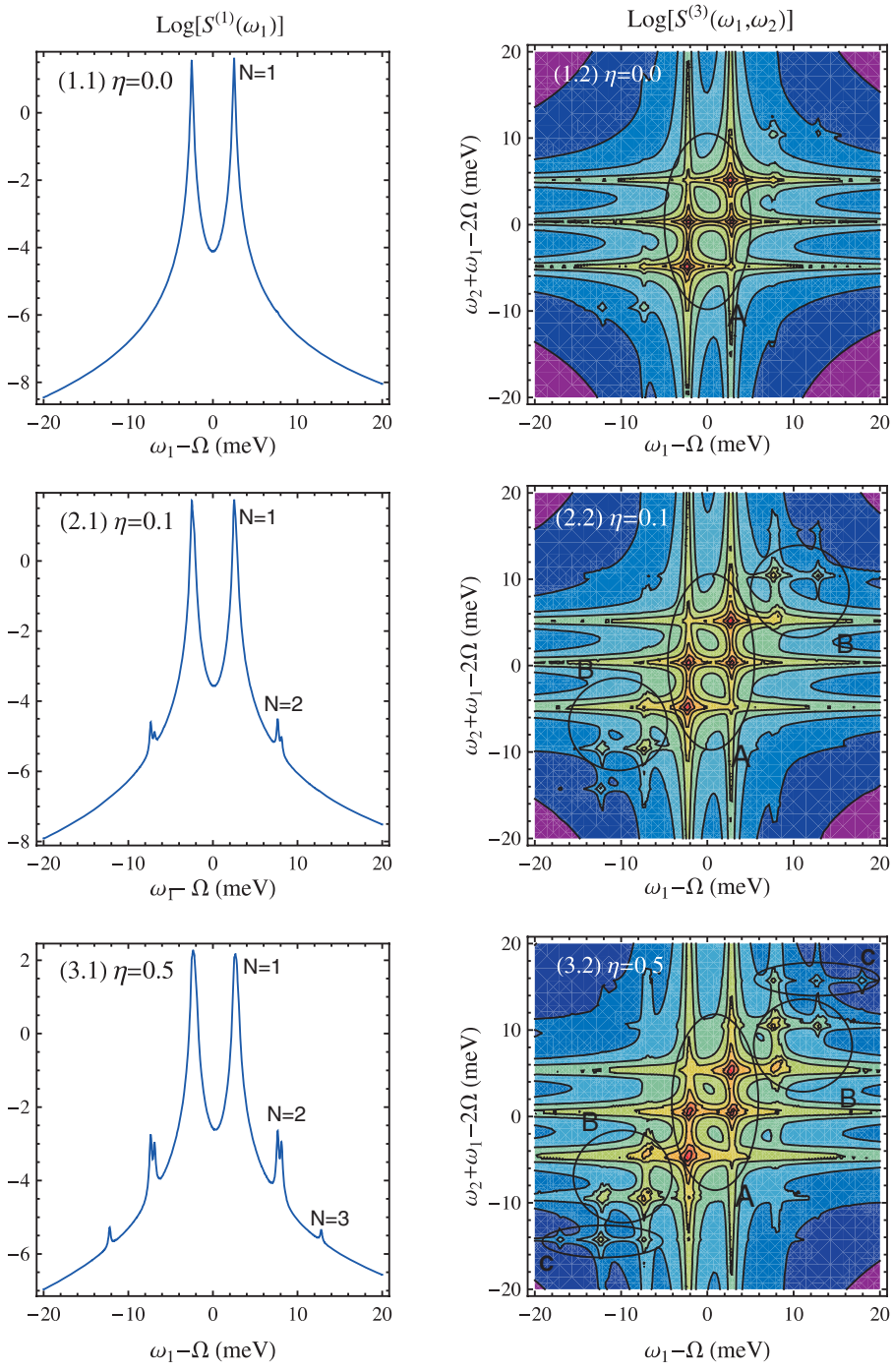

Figure 3. Multi-polariton single (left panels) and two-photon (right panels) fluorescence spectra for small exciton nonlinearities with (2.1), (2.2), (3.1), (3.2) and without CM (1.1), (1.2). Region (C) indicates correlation resonances (CR) between $N=4$ and $N=3$ levels. Region (B) also includes CR from $N=3$ and $N=2$ levels. Region (A) includes, in addition to the above, CR from $N=2$ and $N=1$ levels. (The color version of this figure is included in the online version of the journal.)

detection in solar cells exposed to relatively low intensity sunlight.

5. Conclusions

Using the micro-cavity coupled to weakly confined excitons in quantum dots we investigated the signatures of carrier multiplication in the single- and two-photon emitted frequency resolved fluorescence. These are compared to the spectra provided by the conventional multi-photon induced fluorescence. The two processes are distinguished by the statistics of the initial polariton distribution. We argue that

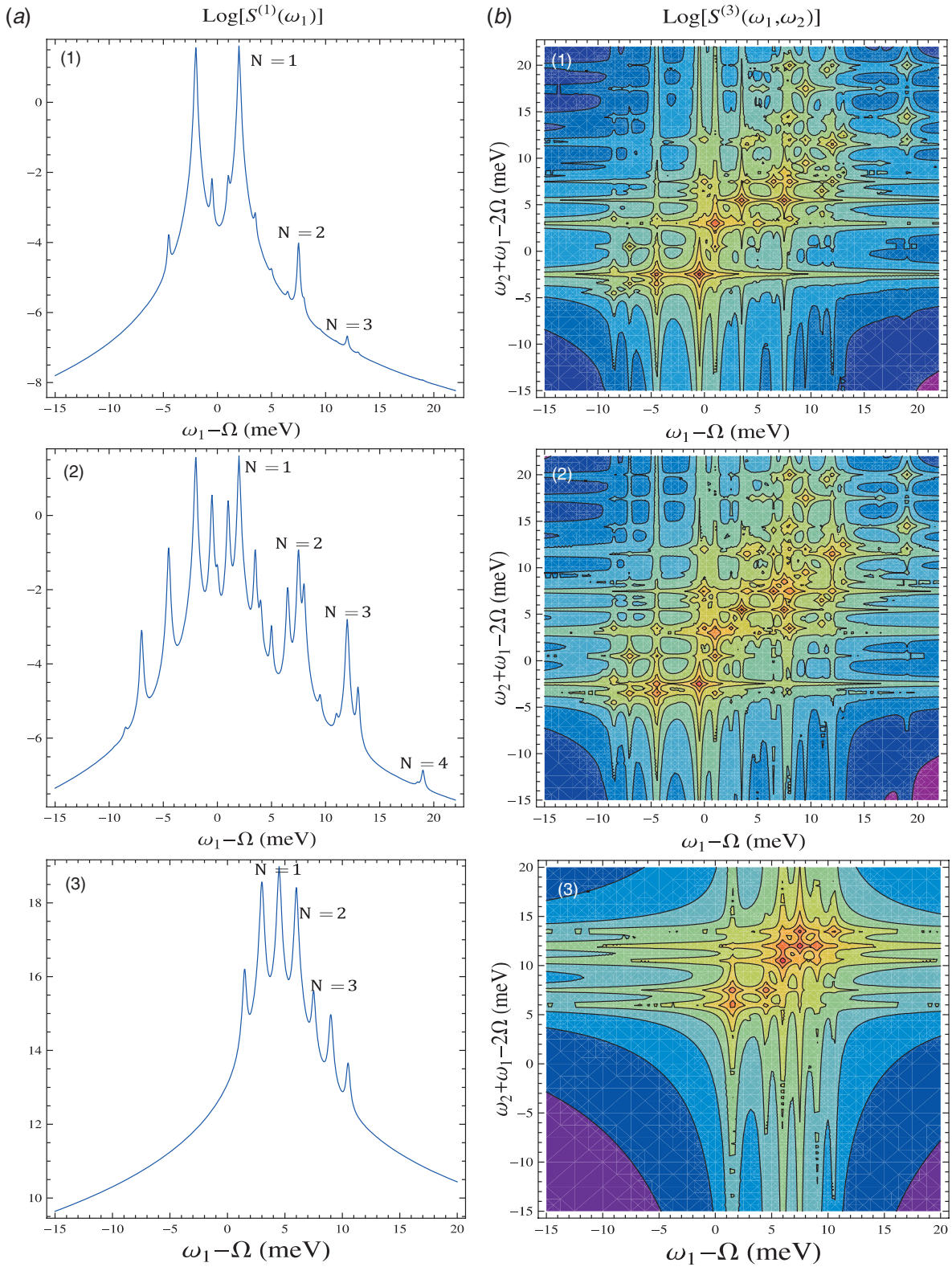

Figure 4. Multi-polariton single (panels (*a*)) and two-photon (panels (*b*)) fluorescence spectra in the presence of exciton nonlinearities comparable with the exciton-photon coupling. Panels (1) show multi-photon induced fluorescence ($\eta = 0$). Panels (2) include CM effect ($\eta = 0.01$) on the spectra. Panels (3) show multi-exciton fluorescence in the absence of the micro cavity coupling (the CM effect is present). Notice that, in the latter case, the presence of CM does not change the spectral form. For all panels the resonances are classified by taking the spectral snapshots along the Auger driven relaxation (see Figure 1(*b*)). (The color version of this figure is included in the online version of the journal.)

exciton emission spectra turned out to be CM insensitive, while the polariton's emission demonstrates strong spectral signatures of the CM. When the polaritonic effect dominates the confinement-boosted exciton's nonlinearities, increasing quantum yield leads to consecutive appearance of Rabi multiplets. The correlation spectra reveals formation of more multiplets as compared with the single photon emission. When the confinement increases, the multiplets start to overlap and their classification requires transient measurements of the spectral snapshots. These are based on the discrete Auger lifetimes of the multi-excitons. Increased nonlinearities boost the CM spectral signatures. According to our model, the search for CM signatures in polariton fluorescence spectra would require smaller pump fluence compared with those for conventional transient photoluminescence.

Acknowledgements

This work was supported by AFRL contract FA 9453-07-C-0207. SM gratefully acknowledges support from the Chemical Sciences, Geosciences and Biosciences Division, Office of Basic Energy Sciences, the Office of Science and the US Department of Energy.

Notes

1. A process whereby the hot electron relaxes to its ground state and the excess energy is transferred via Coulomb scattering to the hole, which is excited deep into the valence band.
2. A highly excited carrier decays to its ground state and excites a valence electron across the bandgap, thus producing two electron-hole pairs from one.
3. We use the term fluorescence rather than photoluminescence since we do not specify the relaxation mechanisms and bundle them up into the dephasing parameter.
4. Since fluorescence is a phase insensitive process, the mode is fully defined by its frequency, and the wave vector may be omitted.

References

[1] Klimov, V. *Annu. Rev. Phys. Chem.* **2007,** *58,* 635–673.
[2] Nozik, A. *Inorg. Chem.* **2005,** *44,* 6893–6899.
[3] McGuire, J.; Joo, J.; Pietryga, J.; Schaller, R.; Klimov, V.I. *Acc. Chem. Res.* **2008,** *41,* 1810–1819.
[4] Klimov, V. *Appl. Phys. Lett.* **2006,** *89,* 123118.
[5] Harrison, D.; Abram, R.A.; Brand, S. *J. Appl. Phys.* **1999,** *85,* 8178–8185.
[6] Nozik, A. *Chem. Phys. Lett.* **2008,** *457,* 3–11.
[7] Velizhanin, K.; Piryatinski, A.; Klimov, V. *Bull. Am. Phys. Soc.* **2010**, 55; Abstr. w14.00001.arXiv:0911.1139v.
[8] Klimov, V. Linear and Nonlinear Optical Spectroscopy of Semiconductor Nanocrystals. In *Handbook of Nanostructured Materials and Nanotechnology*; Nalwa, H.S., Ed.; Academic Press: San Diego, 2000.
[9] Ben-Lulu, M.; Mocatta, D.; Bonn, M.; Banin, U.; Ruhman, S. *Nano Lett.* **2008,** *8,* 1207–1211.
[10] Beard, M.; Knutsen, K.; Yu, P.; Luther, J.; Song, Q.; Metzger, W.; Ellingson, R.; Nozik, A.J. *Nano Lett.* **2007,** *7,* 2506–2512.
[11] Allan, G.; Delerue, C. *Phys. Rev. B* **2008,** *77,* 125340.
[12] Peterson, J.; Krauss, T. *Nano Lett.* **2006,** *6,* 510–514.
[13] Ellingson, R.; Beard, M.; Johnson, J.; Yu, P.; Micic, O.; Nozik, A.; Shabaev, A.; Efros, A. *Nano Lett.* **2005,** *5,* 865–871.
[14] Nair, G.; Bawendi, M.G. *Phys. Rev. B* **2007,** *76,* 081304.
[15] Nair, G.; Geyer, S.M.; Chang, L.Y.; Bawendi, M.G. *Phys. Rev. B* **2008,** *78,* 125325.
[16] Reithmaier, J.; Sek, G.; Loffler, A.; Hofmann, C.; Kuhn, S.; Reitzenstein, S.; Keldysh, L.; Kulakovskii, V.; Reinecke, T.; Forchel, A. *Nature* **2004,** *432,* 197–200.
[17] Yoshie, T.; Scherer, A.; Hendrickson, J.; Khitrova, G.; Gibbs, H.; Rupper, G.; Ell, C.; Shchekin, O.; Deppe, D.G. *Nature* **2004,** *432,* 200–203.
[18] Wu, Z.; Mi, Z.; Bhattacharya, P.; Zhu, T.; Zhu, J. *Appl. Phys. Lett.* **2007,** *90,* 171105.
[19] Beidenharn, L.; Louch, J. *Angular Momentum in Quantum Physics*; Addison-Wesley: London, 1981.
[20] Mukamel, S. *Principles of Nonlinear Optical Spectroscopy*, Oxford University Press: USA, 1995.
[21] Kang, I.; Wise, F. *J. Opt. Soc. Am. B* **1997,** *14,* 1632–1646.
[22] Nimtz, G.; Schlicht, B. *Narrow-gap Lead Salts*; Springer-Verlag: Berlin, 1983.
[23] Inoue, J.I.; Brandes, T.; Shimizu, A. *Phys. Rev. B* **2000,** *61,* 2863–2873.
[24] Takagahara, T. *Phys. Rev. B* **1989,** *39,* 10206–10231.
[25] Khitrova, G.; Gibbs, H.; Jahnke, F.; Kira, M.; Koch, S.W. *Rev. Mod. Phys.* **1999,** *71,* 1591–1639.
[26] Hanamura, E.; Haug, H. *Phys. Rep.* **1977,** *33,* 209.
[27] Marx, C.; Harbola, U.; Mukamel, S. *Phys. Rev. A* **2008,** *77,* 022110.
[28] Hiroshima, T. *Phys. Rev. B* **1989,** *40,* 3862–3866.
[29] Liu, Y.; Imoto, N.; Özdemir, Ş.; Jin, G.; Sun, C.P. *Phys. Rev. A* **2002,** *65,* 023805.
[30] Roslyak, O.; Mukamel, S. *Mol. Phys.* **2009,** *107,* 265–280.
[31] Klimov, V.; Mikhailovsky, A.; McBranch, D.; Leatherdale, C.; Bawendi, M.G. *Science* **2000,** *287,* 1011–1013.
[32] Avancini, S.; Krein, G. *J. Phys. A: Math. Gen.* **1995,** *28,* 685–691.
[33] Liu, Y.X.; Cao, C.Q.; Cao, H. *Phys. Rev. A* **2000,** *61,* 023802.